PROCEEDINGS OF SCIENCE

Cosmic-ray propagation under consideration of a spatially resolved source distribution

Julia Thaler,[a,*] **Ralf Kissmann**[a] **and Olaf Reimer**[a]

[a] *Universität Innsbruck,*
6020 Innsbruck, Austria
E-mail: j.thaler@uibk.ac.at, ralf.kissmann@uibk.ac.at, olaf.reimer@uibk.ac.at

The different elements of the interstellar medium have been continuously sampled through direct and indirect measurements of various messengers, such as cosmic rays (CRs). In addition to observations, numerical simulations of CR propagation, in particular diffuse transport, contribute to understanding the corresponding γ-ray emission components as seen by several experiments. Up to now, the standard approach for modeling source distributions used as input of such transport simulations mostly relies on radial symmetry and analytical functions rather than individual, observation-based sources. We present a redefinition of existing CR source distributions by combining sources observed with the High Energy Stereoscopic System telescope array (H.E.S.S.) and a simulated source distribution, which follows the matter density in the Milky Way. As a result, H.E.S.S.-inspired Galactic CR source distributions are inferred. We use the PICARD code to perform 3D-simulations of particle statistics in CR propagation using our hybrid source distribution models. This implementation of a three-dimensional source model based on observations and simulations enables highly resolved propagation modeling. It opens the path for more realistic CR transport scenarios beyond radial symmetry and delivers improved results in both the arm and interarm regions of the Galaxy. Furthermore, it provides an enhanced picture of the Galactic γ-ray sky including structures from our source model as well as the introduced gas distributions.

38th International Cosmic Ray Conference (ICRC2023)
26 July - 3 August, 2023
Nagoya, Japan

*Speaker

PoS(ICRC2023)352

1. Introduction

Since the discovery of CRs penetrating our Earth's atmosphere, their origin has been constantly investigated. Nowadays, the main Galactic candidates for particle acceleration have been narrowed down to astrophysical object such as supernova remnants or pulsar wind nebulae. However, even with the H.E.S.S. Galactic Plane survey (HGPS) [1] offering the most comprehensive view of the TeV sky in our Galaxy (so far), the resulting source population represents only a small fraction of the contributing Galactic sources. The rest remains hidden under the detection threshold of current instruments, due to their sensitivity and sky coverage. Therefore, the combination of our sparse observed sample with simulated sources offers the possibility to extrapolate our knowledge of a fraction of the Galaxy to the rest of it. In this manuscript we describe the construction of a Galactic CR source model that is based on observations and can be used to simulate CR transport up to describing the diffuse γ-ray sky. The original model was presented in [3], where more detailed information is provided.

2. Construction of the hybrid model

With the premise that most current Galactic source models rely on analytical models and limit themselves to axial symmetry we aim to achieve three dimensional CR source distributions, basing the selection of simulated sources on observations.

As our basis we use the synthetic source population presented in [4]. Its geometry is based on a four-arm spiral Galaxy model and its luminosity distribution on observed source properties from the HGPS, using a large statistical sample of more than two million sources.

As observed sources we mainly use the findings of the HGPS, because it is considered the most comprehensive view of the very-high-energy γ-ray sources in our Galaxy. Still, the resulting source catalogue only represents of a small fraction of the total Galactic source population, since the sensitivity and sky coverage of H.E.S.S. are limited [1]. We get provided with a source catalogue containing 78 firmly identified sources, but only 31 of them have estimated distances from the observer. For the rest we aim to find a counterpart from the simulated source sample [4], assigning them distances. We identify the best fitting simulated source in terms of position in the sky, size and flux to each of our observed sources without distances. To do so we use a k-dimensional tree to assign each HGPS source its nearest neighbours from the simulated sample, staying within a range of 0.1° in Galactic longitude and latitude. Out of this list of potential counterparts we only consider simulated sources with extensions from 70% to 140% of the extension of the observed source. From this sample of possible candidates for each of our HGPS sources we choose the best fitting one by calculating the ratio between the observed flux and the fluxes of all potential simulated sources. We select the source where this ratio is closest to one. This leads to a source sample of 85 observed sources, because we also include some earlier detections like the Galactic center, SN 1006, HESS J0632+057 and the Crab Nebula.

For a realistic modelling of the CR transport in our Galaxy we still want to add additional simulated sources to this observed sample. We only take sources from [4] that would not have been observable by H.E.S.S. into consideration. Therefore, we mask our simulated source sample with the shape of the field of view of the HGPS, to create two sub-samples: one containing all

simulated sources inside and one outside of the field of view of H.E.S.S.. For the sample outside of the field of view there are no further constraints and all the sources can potentially be used for our model, whereas for the sample inside of the field of view we exclude all sources that would have been observed by H.E.S.S.. This is done according to their radial extensions (sources with radial extensions $\alpha > 2^\circ$ are considered to not be detectable) and their fluxes F in comparison to the sensitivity s of H.E.S.S. in their direction, where we consider all sources for which $F < s$ holds. However, this number of potential source candidates is still outnumbering the observed sources and we need to reduce the number of sources in our simulated sample and, therefore, decide on an upper limit for the number of simulated sources. For that we present two different approaches in this work.

The original one is a luminosity approach, it was also used in [3], and defines an upper luminosity limit for the Galaxy. Here we take the upper limit for the expected γ-ray luminosity of our Galaxy of $6.3 \cdot 10^{36}$ ph s^{-1} from [4]. We choose 1%, 10%, 20% and 50% of $6.3 \cdot 10^{36}$ ph s^{-1} as percentile differences from this luminosity limit, as upper boundaries, to investigate the effect of the used percentile difference on the final model. We randomly sample simulated sources until the corresponding luminosity limit is reached. Except for the 50% tolerance model, which only has 631 sources, all the models stay in the same and, according to [4], expected order of magnitude regarding the source numbers, namely between 829 to 925. To increase the amount of observations in our sample we also include the sources from the Fermi catalogue [5], applying a similar search for simulated counterparts as for the HGPS sources without distances, but hereby only relying on Galactic longitude and latitude. With that we find possible simulated counterparts for 137 of the *Fermi* sources and include those into our model.

As a second method, that can be used as a cross-check for the luminosity approach, we use a density approach for the definition of the upper limit. Hereby, we want to extrapolate from known source densities, namely from the HGPS and from the *Fermi* catalogue, to the rest of the Galaxy. For that we use the masking of the field of view, performed before, to extract the area of the HGPS field of view, projected on the x/y-plane. The HGPS source density, $\rho_{\mathrm{HGPS}} = \frac{N_{\mathrm{HGPS}}}{A_{\mathrm{HGPS}}}$, is calculated, from the number of sources inside the field of view of the HGPS N_{HGPS} and the area of the FOV, as the amount of sources per kpc^2 . Since we do not expect to only find very high energy sources we also include sources from the *Fermi* catalogue [5]. The *Fermi* sources are correspondingly divided into *Fermi* sources inside and outside of the H.E.S.S. field of view. This gives us $N_{\mathrm{FERMI,in}}$ and $N_{\mathrm{FERMI,out}}$. We expect to find additional $N_{\mathrm{FERMI,in}}$ simulated sources in the field of view of the HGPS and $N_{\mathrm{out}} = N_{\mathrm{HGPS,out}} + N_{\mathrm{FERMI,out}}$ simulated sources outside of the FOV. We randomly pick sources according to those expected numbers from the corresponding simulated sub-samples. The sources number we derive from this approach is again within the expected range from 800 to 7000 sources[4], with 869 sources and the total luminosity $5.33 \cdot 10^{36}$ ph s^{-1} is also close to the upper luminosity limit of our Galaxy [4].

This leaves us with a total set of nine models: Luminosity approach with HGPS only ($LA_{1\%}$, $LA_{10\%}$, $LA_{20\%}$, $LA_{50\%}$) and with HGPS and *Fermi* data ($LAF_{1\%}$, $LAF_{10\%}$, $LAF_{20\%}$, $LAF_{50\%}$) and density approach (DA).

2.1 Radial distribution of the CR sources in the hybrid models

The radial distribution of CR sources in the Galaxy has been studied thoroughly and suits as an indicator for the plausibility of our source models. We compare our models with previously studied distributions ([7], [6], [8]), which all show a steep decrease towards the Galactic center to almost zero sources. Our models also show lower surface densities in the Galactic center region (see figure 1), which can be related to the absence of a Galactic bar in the underlying simulated sample [4]. The radial distributions (figure 1) shows that a percentile difference of 50% of the upper luminosity

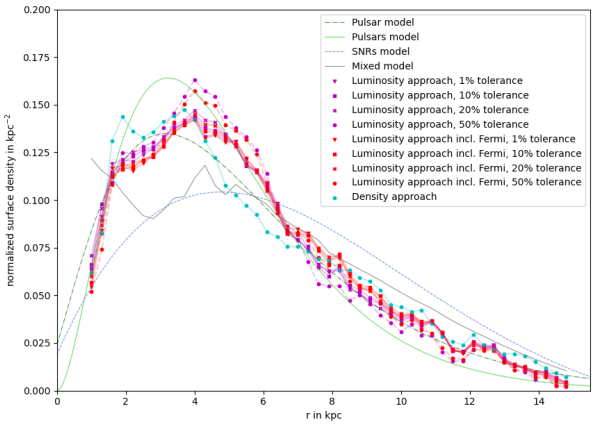

Figure 1: CR source densities as a function of Galactocentric radius. We show distributions for the models using the luminosity approach with only HGPS sources in magenta, the luminosity approach also including the Fermi sources in red and the density approach is shown in cyan. We also show some radial distribution from the literature (top to botton in the legend: [7], [6], [8], [9]).

limit results in a higher source density, whereas the other differences all stay in the same range. In comparison to the density approach we can see that the latter shows lower source numbers within the field of view because we constrain the random sampling to not go over $N_{\mathrm{FERMI,\ in}}$ there, while in the luminosity approach we sample uniformly from all the Galaxy.

3. Cosmic-ray transport simulation and results

Our new source models are implemented for use in the *Picard* code, which is computing steady state solutions for CR transport. For a detailed description of the framework see [2] and for the transport parameters we used we refer to [3]. Alfven speed and diffusion coefficient have been tuned separately to fit the observed spectra at Earth, as shown in figure 2. The secondary to primary ratios of our models fit the observations at Earth, within the errors. However, we can see that some of our models fit better than others. Furthermore, figure 2 shows that in principle all our models, mostly discriminating between with and without *Fermi* sources, would require slightly different transport parameters, also because they contain different energy regimes and source spectra. However, for the comparison of the different luminosity limits we kept the parameters constant for all simulations.

The input parameters for each source in the simulation consist not only of its three-dimensional position but also contain fluxes, source classes, spectral information and energy ranges. Where the

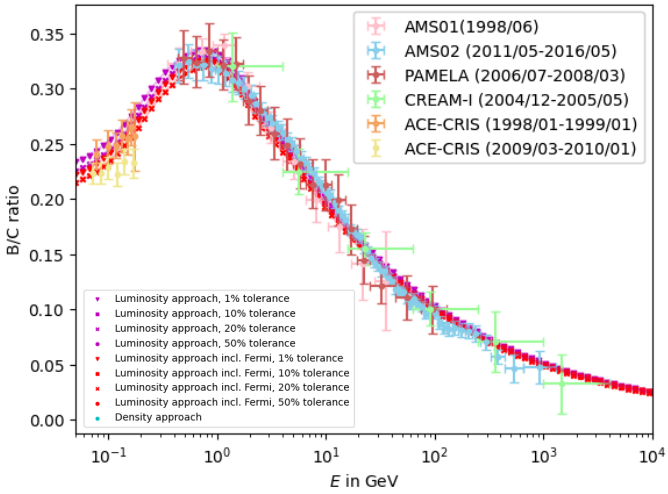

Figure 2: B/C-ratio for our luminosity approach models with the different tolerances with and without FERMI-sources and the density approach model in comparison with CR data taken from different experiments (top to bottom in legend: [10], [11], [12], [13], [14], [15].

last three have been assumed to have the same ratios as in our observed distributions. With those parameters we can simulate CR density distributions and particle spectra as well as a synthetic γ-ray sky. The density distributions are shown for electrons and protons in figure 3.

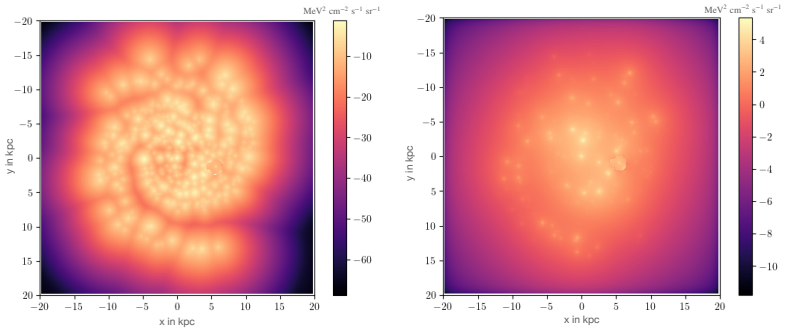

Figure 3: *Right*: Density distribution of simulated CR electrons at an energy of 10 TeV in the x/y-plane of the Galaxy, using the distribution of the luminosity approach model with 20% tolerance and without *Fermi* sources, exemplarily. The Solar System is located at $(8.5, 0)$ kpc and the distribution is shown in a logarithmic scale for better visibility. *Left*: Same but for protons.

We show the proton and electron spectral intensities from our models together with corresponding CR observations in figure 4. In the electron spectra (left side of figure 4), it is visible that all our models except for the luminosity approach with 1% percentile difference fit the observed data in the high energy regime. In the lower energy regime simulations do not fit the observations as the experimental data is higher than our synthetic spectra. This could be improved by adding more low energetic leptonic sources to our model, for example by including the Fermi Pulsar catalogue [25].

With the *Picard* code we also simulate γ-ray emissivities and fluxes, which is done separately

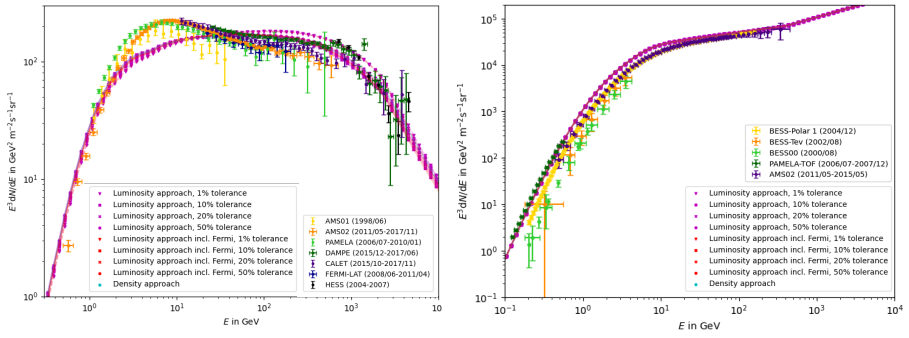

Figure 4: *Left*: Electron spectra for our models for the four different tolerances in the luminosity approach, both with and without the *Fermi* sources as well as the density approach model with observed data from different experiments (top to bottom in the legend: [10], [11], [17], [23], [24], [16], [18] *Right*: Same but for CR protons. Experiments top to bottom: [20], [21], [19], [22].

by line-of-sight-integration for the relevant radiation processes. In figure 5 we show an exemplary simulation for one of our models, for both inverse Compton scattering and the total γ-emission. On the right side of figure 5 we can clearly see the impact of the source distribution on the inverse Compton γ-ray sky, since it is dominated by CR electrons and, therefore, the fluxes peak at the corresponding sources.

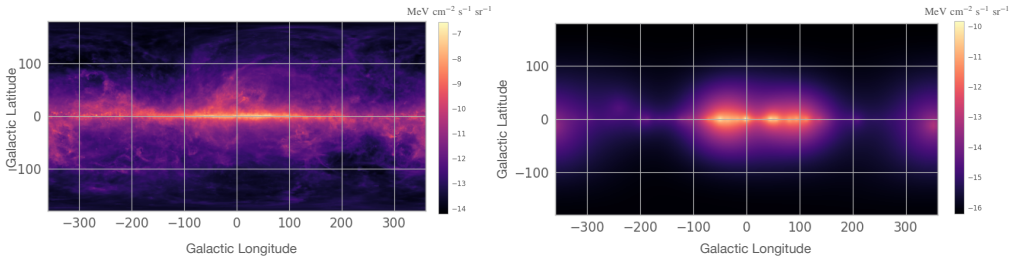

Figure 5: *Right*: Total γ-ray flux at an energy of 1 TeV (luminosity approach model with 20% tolerance and without *Fermi* sources as an example. *Left*: Same but for inverse Compton scattering.

4. Conclusion

In conclusion we can say that both the luminosity and the density approach are able to reproduce measured CR quantities, like the secondary to primary ratio and particle spectra. We note that the different upper limits applied to the luminosity approach affect our random source selection and have impacts on the subsequent simulations. Therefore, we can say that a tolerance of 20% gives us the most continuously fitting results. This also leads to a more constrained guess on the upper limit of the total luminosity we expect the Milky Way to have. Moreover, the density approach model is in coherence with observations and with the luminosity approach, which is an additional cross-check on the luminosity limit. However, in the resulting particle spectra we can see some improvement potential, namely for example in the inclusion of other data, like the FERMI pulsar catalogue [25], which can be addressed in future studies.

References

[1] H.E.S.S. Collaboration, H. Abdalla, A. Abramowski, F. Aharonian, F. Ait Benkhali, E.O. Angüner et al. (2018), *The H.E.S.S. Galactic plane survey*

[2] R. Kissmann (2014), *PICARD: A novel code for the Galactic Cosmic Ray propagation problem*

[3] J. Thaler, R. Kissmann, O. Reimer (2022), *Cosmic-ray propagation under consideration of a spatially resolved source distribution*

[4] C. Steppa, K. Egberts (2020), *Modelling the galactic very-high-energy gamma-ray source population*

[5] FERMI Collaboration, S. Abdollahi, F. Acero, L. Baldini, J. Ballet, D. Bastieri et al. (2022), *Incremental FERMI Large Area Telescope Fourth Source Catalog*

[6] D. R Lorimer, A. J. Faulkner, A. G. Lyne, R. N. Manchester, M. Kramer et al. (2006), *The Parkes Multibeam Pulsar Survey - VI. Discovery and timing of 142 pulsars and a Galactic population analysis*

[7] I. Yusifov, I. Küçük (2004), *Revisiting the radial distribution of pulsars in the Galaxy*

[8] G. L. Case, D. Bhattacharya (1998), *A new sigma-D relation and its application to the galactic supernova remnant distribution*

[9] E. Carlson, T. Linden, S. Profumo (2016), *Improved cosmic-ray injection models and the Galactic Center gamma-ray excess*

[10] M. Aguilar, J. Alcaraz, J. Allaby, B. Alpat, G. Ambrosi et al. (2010), *Relative composition and energy spectra of light nuclei in cosmic rays: results from AMS-01*

[11] M. Aguilar, L. Ali Cavasonza, G. Ambrosi, L. Arruda, N. Attig et al. (2010), *Precision Measurement of the Boron to Carbon Flux Ratio in Cosmic Rays from 1.9 GV to 2.6 TV with the alpha magnetic spectrometer on the international space station*

[12] O. Adriani, G.C. Barbarino, G.A. Bazilevskaya, R. Bellotti, M. Boezio et al. (2014), *Measurement of boron and carbon fluxes in cosmic rays with the PAMELA experiment*

[13] H. Ahn, P. Allison, M. Bagliesi, J. Beatty, G. Bigongiari et al. (2008), *Measurements of cosmic-ray secondary nuclei at high energies with the first flight of the CREAM balloon-borne experiment*

[14] G. de Nolfo, I. Moskalenko, W. Binns, E. Christian, A. Cummings et al. (2006), *Observations of the Li, Be, and B isotopes and constraints on cosmic-ray propagation*

[15] K.A. Lave, M. E. Wiedenbeck, W. R. Binns, E. R. Christian, A. C. Cummings et al. (2013), *Galactic cosmic-ray energy spectra and composition during the 2009–2010 solar minimum period*

[16] Fermi LAT Collaboration, M. Ackermann, M. Ajello, A. Allafort, W. B. Atwood, L. Baldini et al. (2012), *Measurement of separate cosmic-ray electron and positron spectra with the Fermi large area telescope*

[17] O. Adriani, G.C. Barbarino, G. A. Bazilevskaya, R. Bellotti, M. Boezio et al. (2011), *Cosmic-ray electron flux measured by the PAMELA experiment between 1 and 625 GeV*

[18] F. Aharonian, A. G. Akhperjanian, U. Barres de Almeida, A. R. Bazer-Bachi, Y. Becherini et al. (2008), *Energy spectrum of cosmic-ray electrons at TeV energies*

[19] O. Adriani, G. C. Barbarino, G. A. Bazilevskaya, R. Bellotti, M. Boezio et al. (2016), *Measurements of cosmic-ray hydrogen and helium isotopes with the PAMELA experiment*

[20] K. Abe, H. Fuke, S. Haino, T. Hams, A. Itazaki et al. (2008), *Measurement of the cosmic-ray low-energy antiproton spectrum with the first BESS-Polar Antarctic flight*

[21] Y. Shikaze, S. Haino, K. Abe, H. Fuke, T. Hams et al. (2007), *Measurements of 0.2–20 GeV/n cosmic-ray proton and helium spectra from 1997 through 2002 with the BESS spectrometer*

[22] M. Korsmeier, A. Cuoco (2017), *Galactic cosmic-ray propagation in the light of AMS-02: I. Analysis of protons, helium, and antiprotons*

[23] DAMPE Collaboration, G. Ambrosi, Q. An, R. Asfandiyarov, P. Azzarello, P. Bernardini et al. (2017), *Direct detection of a break in the teraelectronvolt cosmic-ray spectrum of electrons and positrons*

[24] O. Adriani, Y. Akaike, K. Asano, M. G. Bagliesi, G. Bigongiari et al. (2017), *Energy Spectrum of Cosmic-ray Electron and Positron from 10 GeV to 3 TeV Observed with the Calorimetric Electron Telescope on the International Space Station*

[25] Fermi LAT Collaboration (2013), *The Second Fermi Large Area Telescope Catalog of Gamma-ray Pulsars*

PoS(ICRC2023)352